Formulae of Maximum Stresses and Tensile Stiffnesses for Rectangular Array and Zig-zag Array of Elliptical Holes in Solids under Uniaxial Tension

Hidenobu IGAWA*

Abstract

This paper is concerned with theoretical analyses of a rectangular array and a zig-zag array of elliptical holes in solids under uniaxial tension. In the analyses, we choose suitable unit regions, and express Laurent series expansions for the complex potentials in forms satisfying the traction-free conditions along the elliptical hole edges. Then the unknown coefficients in the Laurent series are determined from the boundary conditions at the outer edges of the used unit regions. At this stage, we use a procedure based on element-wise resultant forces and displacements in order to get highly accurate results. Numerical results of the maximum stresses represented in dimensionless forms in the whole range of the shapes of the holes including cracks, and the tensile stiffnesses of the solids with the holes, are given for various values of the parameters. The results are fitted to reliable polynomial formulae for convensience of engineering applications.

Key words: Two-Dimensional Elasticity, Tension, Stress Concentration, Stress Intensity Factor, Tensile Stiffness, Elliptical Holes, Cracks

1. Introduction

Holes are found in many natural and manufactured solid materials, and their effects on the structural behavior of solids are of continuing concern. In particular, the presence of the holes causes weakening and apparent lowering of Young's modulus of the materials. Therefore, in order to use the engineering structures safely, we should estimate the exact strength and stiffness of the materials with the holes.

In this paper, we consider a rectangular array and a zig-zag array of elliptical holes in solids under uniaxial tension as two-dimensional models of randomly distributed holes in materials.

In the analyses, we choose suitable unit regions, and express Laurent series expansions for the complex potentials in forms satisfying the traction-free conditions along the elliptical hole edges. Then the unknown coefficients in the Laurent series are determined from the boundary conditions at the outer edges of the used unit regions. At this stage, we use a new procedure based on element-wise resultant forces and displacements in order to get highly accurate results. This method was developed by Isida[3] and has proven a powerful technique both in plane problems and three-dimensional problems[4]. Numerical calculations are carried out for various shapes, sizes, and square systems of the elliptical holes in solids. The analytical values are then fitted to reliable polynomial formulae for convenience of engineering applications.

*機械工学科
平成11年9月30日受理

2. Theoretical analysis

2. 1. *Complex stress potentials*

In plane problems of elasticity, the Cartesian components of stress, reslutant force and displacement are given in terms of two complex potentials $\varphi(z)$, $\psi(z)$ as follows:

$$\sigma_y+\sigma_x=4\varphi'(z)$$

$$\sigma_y-\sigma_x+2i\tau_{xy}=2[\bar{z}\varphi''(z)+\psi''(z)] \tag{1}$$

$$P_y+iP_x=-\bar{\varphi}(\bar{z})-\bar{z}\varphi'(z)-\psi'(z) \tag{2}$$

$$2G(u-iv)=\varkappa\bar{\varphi}(\bar{z})-\bar{z}\varphi'(z)-\psi'(z), \tag{3}$$

where G is the shear modulus and $\varkappa$ is defined by Poisson's ratio ν as

$$\varkappa=\begin{cases}\dfrac{3-\nu}{1+\nu} & \text{(plane stress)}\\ 3-4\nu & \text{(plane strain)}.\end{cases} \tag{4}$$

This paper deals with the following two typical distributions of elliptical holes in an infinite solid subjected to uniaxial tension:

Problem (a): Rectangular array of elliptical holes (Fig. 1(a))

Problem (b): Zig-zag array of elliptical holes (Fig. 1(b)).

In both the problems, let $2a$ and $2b$ be the major and minor diameters, ρ be the radius of curvature at the end of the major axes of the elliptical holes, and b, c be the spacings in the directions parallel and vertical to the load, respectively, as shown by Figs. 1(a) and 1(b). The x- and y-axes are taken with their origin at the center of one of the elliptical holes, and the solids are subjected to an average tensile stress σ in the y-direction.

2. 2. *Laurent series expansions of complex stress potentials*

We take proper unit regions and express the complex stress potentials in forms satisfying the symmetry conditions of the stress state, as well as the traction-free conditions along the elliptical hole edges. We then determine the unknown coefficients in the stress potentials from the boundary conditions at the outer edges of unit regions.

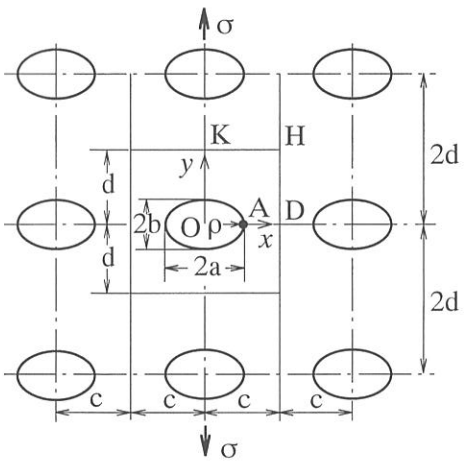

Fig. 1(a)　Rectangular array of elliptical holes

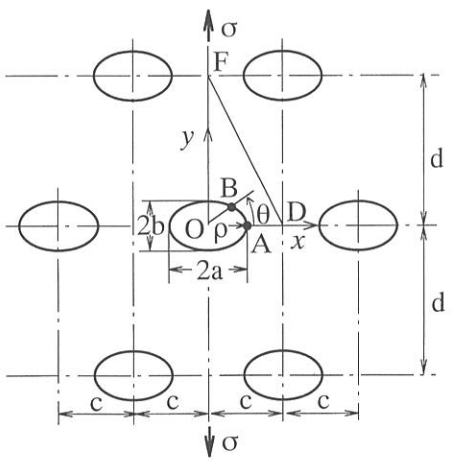

Fig. 1(b)　Zig-zag array of elliptical holes

For the above unit regions, we have chosen the rectangle ODHKO for Problem (a) and the triangle ODFO for Problem (b) shown in Figs. 1(a) and 1(b), noting the symmetry of stress field about both the coordinates' axes.

The complex potentials $\varphi(z)$, $\psi(z)$ must be analytic in the unit region, and they can be expanded in the following Laurent series:

$$\varphi(z)=\sum_{n=0}^{\infty}(G_{2n}z^{-2n-1}+M_{2n}z^{2n+1})$$

$$\psi(z)=-D_0\log z+\sum_{n=0}^{\infty}(D_{2n+2}z^{-2n-2}+K_{2n}z^{2n+2}), \tag{5}$$

where G_{2n}, M_{2n}, D_{2n}, K_{2n} are real coefficients. The complex potentials (5) also satisfy the conditions of symmetry of the stress state about the x- and y-axes.

Since the elliptical hole is traction-free, some relations must exist among the coefficients of the Laurent series (5). These relations were given by Isida[1][2] as follows:

$$D_{2n}=\sum_{p=0}^{\infty}a^{2n+2p+2}(P_{2p}^{2n}K_{2p}+R_{2p}^{2n}M_{2p})$$

$$G_{2n}=-\sum_{p=0}^{\infty}a^{2n+2p+2}(Q_{2p}^{2n}K_{2p}+S_{2p}^{2n}M_{2p}) \tag{6}$$

where P_{2p}^{2n} etc. are constants given by $b/a(=\sqrt{\rho/a})$, the ratio of the shape of the elliptical hole.

2. 3. Boundary conditions and determination of unknowns

The complex potentials (5), rewritten in terms of the independent unknowns K_{2n} and M_{2n} using eqn (6), completely satisfy the traction-free conditions along the elliptical hole edges, as well as the symmetry conditions of the stress state in the x and y directions. Therefore, the unknown coefficients K_{2n} and M_{2n} must be determined only from the boundary conditions along the sides DF and FK for the rectangular unit region in Fig. 2, or along the side DF for the triangular unit region in Fig. 3.

For the numerical calculation, we use a method based on element-wise resultant forces and displacements. This method was developed by Isida[3][5] and proved a powerful technique in analyzing various problems of multi-connected regions. The procedures for both the problems will be described below.

(a) *Rectangular array of elliptical holes* [Fig. 2]

We divide the sides DH and HK of the rectangular unit region into N_1 and N_2 equal intervals, respectively. These intervals are Q_1Q_2, Q_2Q_3, $\cdots$ and Q_NQ_{N+1} $(N=N_1+N_2)$, as shown in Fig. 2.

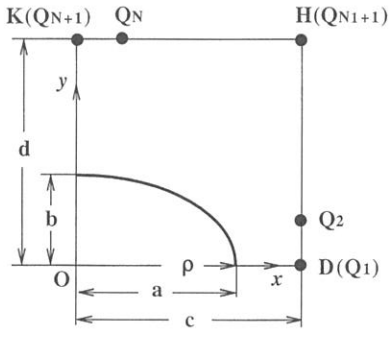

Fig. 2 Rectangular unit region

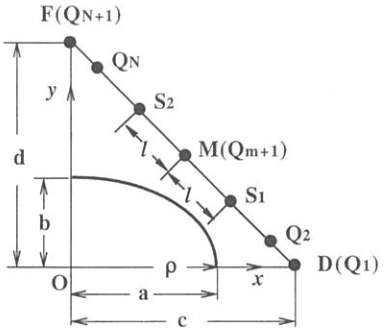

Fig. 3 Triangular unit region

Side DH:

The stress state is symmetric about DH, that is: τ_{xy} vanishes and u is constant along DH. These conditions are replaced by the following relations in terms of P_y and u for each of the intervals:

$$[P_y]_j=0 \ (j=1, 2, \cdots, N_1)$$
$$[u]_{j+1}-[u]_j=0 \ (j=1, 2, \cdots, N_1-1), \tag{7}$$

where j is the interval number. $[P_y]_j$ is given from the real part of eqn (2) by taking the difference of P_y at the two points Q_{j+1} and Q_j, and $[u]_j$ is defined by the mean of u at Q_{j+1} and Q_j which are obtained from the real part of eqn (3), that is

$$[P_y]_j=P_{y,\,Q_{j+1}}-P_{y,\,Q_j}$$
$$[u]_j=(u_{Q_{j+1}}+u_{Q_j})/2 \ (j=1, 2, \cdots, N_1) \tag{8}$$

Side HK:

The stress state is symmetric about side HK, and we have the following relations similar to eqn (7):

$$[P_x]_j=0 \ (j=N_1+1, N_1+2, \cdots, N)$$
$$[v]_{j+1}-[v]_j=0 \ (j=N_1+1, N_1+2, \cdots, N-1), \tag{9}$$

where $[P_x]_j$, $[v]_j$ are defined as

$$[P_x]_j=P_{x,\,Q_{j+1}}-P_{x,\,Q_j}$$
$$[v]_j=(v_{Q_{j+1}}+v_{Q_j})/2 \ (j=N_1+1, N_1+2, \cdots, N). \tag{10}$$

Furthermore, the resultant forces along DH and HK should balance the external load, and we have

$$[P_x]_D^H=0, \ ]P_y]_H^K=\sigma c. \tag{11}$$

(b) *Zig-zag array of elliptical holes* [Fig. 3]

Let M be the mid-point of side DF. So the stress field is symmetric about M, and any two points S_1 and S_2 on DF which are equidistant from M(l) must be in the same stress state and displacements of these points relative to M must be the same. These boundary conditions lead to the following relations:

$$[P_x]_{Q_t}^{Q_{m+1}}=[P_x]_{Q_{m+1}}^{Q_{2m+2-t}}$$
$$[P_y]_{Q_t}^{Q_{m+1}}=[P_y]_{Q_{m+1}}^{Q_{2m+2-t}} \ (t=1, 2, \cdots, m;\ m=N/2) \tag{12}$$
$$[u]_{Q_t}^{Q_{m+1}}=[u]_{Q_{m+1}}^{Q_{2m+2-t}}$$
$$[v]_{Q_t}^{Q_{m+1}}=[v]_{Q_{m+1}}^{Q_{2m+2-t}} \ (t=1, 2, \cdots, m;\ m=N/2) \tag{13}$$

Furthermore, the resultant forces along the outer edges of the unit region should balance the external load, and we have

$$[P_x]_D^F=0, \ [P_y]_D^F=\sigma c. \tag{14}$$

Thus we have $2N$ relations by eqns (7), (9), (11) for Problem (a), and $(2N+2)$ relations by eqns (12), (13), (14) for Problem (b). Corresponding to these relations, we take $2N$ unknowns $K_{2n}(n\leq N)$, $M_{2n}(n\leq N)$ for Problem (a) and $(2N+2)$ unknowns $K_{2n}(n\leq N+1)$, $M_{2n}(n\leq N+1)$ for Problem (b) neglecting higher order coefficients, and these unknowns are determined from the corresponding boundary conditions shown above.

3. Numerical results and discussions

3. 1. Physical quantities and accuracy of results

Numerical results of the treated problems depend upon the ratio of a, b, c and d, or upon the three dimensionless parameters below:

$$\mu=\frac{c}{b}, \ \lambda=\frac{a}{c}, \ \varepsilon=\frac{b}{a}=\sqrt{\frac{\rho}{a}} \tag{15}$$

Table 1 Variations of results with subdivision numbers

N	Problem (a) ($c/d=1$, $a/c=0.8$, $\rho/a=0.25$, rectangular unit region)		Problem (b) ($c/d=1$, $a/c=0.6$, $\rho/a=0.25$, triangular unit region)	
	σ_A/σ	E^*/E_0	σ_A/σ	E^*/E_0
8	7.9465	0.3533	7.9305	0.2291
16	7.9251	0.3535	7.9284	0.2292
24	7.9251	0.3536	7.9283	0.2292
32	7.9251	0.3536	7.9283	0.2292

In the present problem, we are especially interested in two quantities. One is the distribution of tangential stress σ_t along the hole, and other is the effect of holes on the apparent tensile stiffness of te solid. With reference to the latter quantity, the followig dimensionless factor C is defined:

$$C=\frac{E^*}{E_0}=\text{tensile stiffness factor}$$

E^*=apparent Young's modulus of solid with elliptical holes

E_0=Young's modulus of material

$$=\begin{cases} E & \text{(plane stress)} \\ E/(1-\nu^2) & \text{(plane strain)} \end{cases}, \tag{16}$$

where E is Young's modulus of the material measured with thin plate specimens. E^* and E_0 depend on E and ν, but $C=E^*/E_0$ is independent of them and is common to the plane stress and the plane strain cases.

Numerical results from the present analyses are expected to approach the exact values with increasing numbers of the boundary elements of the used unit regions, or N. As an example, Table 1 gives σ_A/σ and E^*/E_0 with various values of N when $c/d=1$, $a/c=0.8$ and $\rho/a=0.25$ for Problem (a), and $c/d=1$, $a/c=0.6$ and $\rho/a=0.25$ for Problem (b). σ_A is the tangential stress at point A on the hole edge as shown in Figs. 1(a) and 1(b). We find rapid convergence of the results with increasing subdivision numbers.

It would consume an enormous number of pages to present here all the numerical results for a number of combinations of the parameter μ. For this reason, we take a square array ($\mu=1$) for Problem (a) and zig-zag array ($\mu=1$) for Problem (b) as special distributions of the elliptical holes in solids. The procedure as shown in Table 1 has been taken to confirm high accuracy of all the numerical results to be discussed in the following sections.

3. 2. Stress magnification factors and their formulae

In Problem (a), σ_{max}, the maximum stress around the hole, occurs at point A as shown in Fig. 1(a). In Problem (b), σ_{max} occurs at point A($\theta=0$) in most of the calculated cases of ε and λ, but in some cases of ε and λ, σ_{max} takes place at some other point B($\theta\neq0$) due to interference by the presence of obliquely located holes. We show such a case in Fig. 4.

In representing these stresses, we use the following dimensionless factors S_A and S_B:

$$S_A=\frac{\sigma_A}{\sigma_0},\ S_B=\frac{\sigma_B}{\sigma_0} \tag{17}$$

where σ_0 is the maximum stress for a single elliptical hole in a wide plate subjected to tension, that is

$$\sigma_0=\sigma\left(1+2\sqrt{\frac{a}{\rho}}\right)=\sigma\left(1+2\frac{a}{b}\right). \tag{18}$$

The above dimensionless quantities represent the stress magnification effect due to interactions among the holes, and

are convenient in the whole range of the hole shapes including cracks. Actually in the case of cracks ($\rho \to 0$), σ_A and σ_B diverge towards infinity, but S_A and S_B remain finite and are equal to the dimensionless stress intensity factors based on $\sigma\sqrt{\pi a}$, that is

$$(S_A)_{\rho\to 0}=(S_B)_{\rho\to 0}=\frac{K_{I,A}}{\sigma\sqrt{\pi a}}. \tag{19}$$

The maximum dimensionless stress S_{max} corresponding to the maximum stress is then defined as follows:

$$S_{max}=\max(S_A, S_B). \tag{20}$$

Numerical calculations have been carried out for the combinations of the following values of the parameters; $\mu=1$ (square array), $\varepsilon=0$ (cracks), 0.2, 0.4, 0.5, 0.6, 0.8, 1 (circular holes), 1.5, 2, 3, 4 and $\lambda=0$, 0.1, 0.2, ··· for Problem (a); $\mu=1$, $\varepsilon=0$ (cracks), 0.2, 1/3, 0.4, 0.5, 0.6, 0.8, 1 (circular holes), 1.5, 2, 3, 4 and $\lambda=0$, 0.1, 0.2, ··· for Problem (b). Results of the dimensionless quantities defined by eqns (16)-(20) are plotted in Fig. 5(a) to Fig. 8(b), where symbols '(a)' and '(b)' correspond to Problem (a) and Problem (b) throughout all the following figures and tales.

Table 2(a), (b) show the numerical results of S_{max} for various values of ε and λ. In most of the calculated cases, σ_A gives the maximum tangential stress along the hole edge, but not in the range bounded by the dotted line shown in Table 2(b). In this range, σ_B occurs at the some other point B($\theta \neq 0$) along the hole edge, as shown in Fig. 4. The values of S_{max} and their locations θ (in degrees) are also given in Table 2(b).

The values of S_{max} for Problem (a) and Problem (b) are plotted by thick solid curves in Fig. 5(a) and 5(b), respectively. The thin solid curves in Fig. 5(b) show S_A in the range where $S_A < S_{max}$.

S_{max} for Problem (a) is given by S_A, and S_{max} - curves for the calculated cases of ε increases monotonically as λ increases and diverges towards infinity when $\lambda \to 1$.

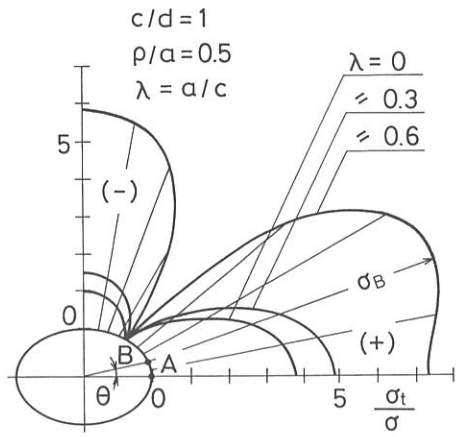

Fig. 4　Distribution of σ_t/σ (Problem (b))

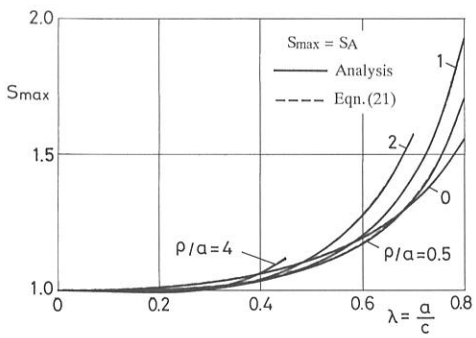

Fig. 5(a)　S_{max} for Problem (a) ($c/d=1$)

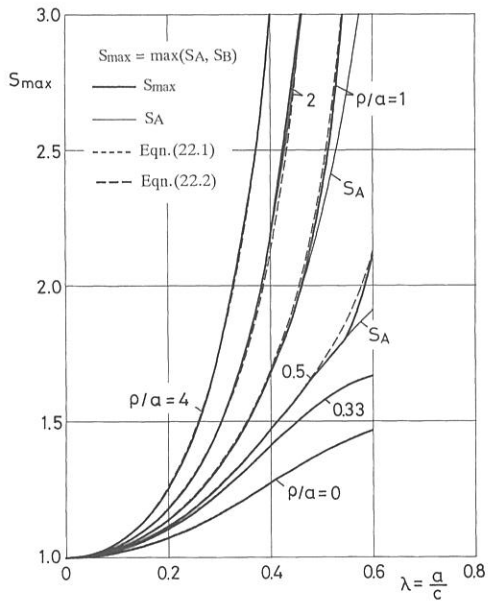

Fig. 5(b)　S_{max} for Problem (b) ($c/d=1$)

Table 2(a) S_{max} for Problem (a) ($c/d=1$)

a/c	ρ/a									
	0	0.2	0.4	0.5	0.6	0.8	1.0	1.5	2.0	4.0
0.0	1.000	1.000	1.000	1.000	1.000	1.000	1.000	1.000	1.000	1.000
0.1	1.003	1.001	1.001	1.001	1.000	1.000	1.000	0.999	0.999	0.997
0.2	1.012	1.007	1.005	1.004	1.003	1.002	1.001	0.999	0.998	0.994
0.3	1.031	1.019	1.016	1.014	1.013	1.011	1.010	1.008	1.006	1.008
0.4	1.062	1.045	1.040	1.039	1.038	1.037	1.036	1.037	1.041	1.065
0.5	1.113	1.090	1.087	1.086	1.087	1.089	1.093	1.106	1.121	
0.6	1.194	1.166	1.168	1.172	1.177	1.189	1.203	1.239	1.276	
0.7	1.324	1.296	1.319	1.335	1.351	1.386	1.421	1.502	1.574	
0.8	1.558	1.563	1.657	1.706	1.753	1.843	1.924	2.097		

Table 2(b) S_{max} for Problem (b) ($c/d=1$)

a/c	ρ/a											
	0	0.2	1/3	0.4	0.5	0.6	0.8	1.0	1.5	2.0	3.0	4.0
0.0	1.000	1.000	1.000	1.000	1.000	1.000	1.000	1.000	1.000	1.000	1.000	1.000
0.1	1.018	1.024	1.026	1.027	1.028	1.029	1.031	1.033	1.037	1.041	1.047	1.052
0.2	1.073	1.097	1.106	1.110	1.115	1.120	1.130	1.139	1.160	1.179	1.217	1.253
0.3	1.162	1.218	1.240	1.250	1.265	1.280	1.309	1.339	1.413	1.489	1.640	1.772
0.4	1.273	1.365	1.411	1.434	1.470	1.508	1.588	1.677	1.921	2.177	2.641	3.007
0.5	1.383	1.491	1.572	1.619	1.699	1.789	2.019 (11°)	2.335 (17°)	3.285 (23°)	4.383 (26°)		
0.6	1.468	1.546	1.669	1.789 (9°)	2.111 (15°)	2.532 (18°)	3.643 (24°)	5.238 (27°)	14.98 (33°)			

( ) : Location θ (in degree) of σ_{max} occuring at the point B.

S_{max} for Problem (b) is given by S_A in wide range of λ, and increase monotonically with increasing values of λ. However, S_{max} for large values of λ shows the different tendency of diverge due to the interference between adjacent holes, depending on the three ranges of ε as shown in Fig. 6 (i -iii). Thus, when $0\leq\varepsilon<1/3$, the horizontally adjacent holes touch each other as shown in Fig. 6(i). In such cases, S_{max} is given by S_A and diverges towards infinity when $\lambda\to1$. When $1/3<\varepsilon<3$, the obliquely adjacent holes touch each other when $\lambda=\sqrt{\varepsilon^2+1}/(2\varepsilon)$ as shown in Fig. 6(ii). In such cases, S_{max} is given by S_B as the values of λ get larger than $\lambda=0.4\sim0.5$ and diverges towards infinity when $\lambda\to\sqrt{\varepsilon^2+1}/(2\varepsilon)$. When $\varepsilon>3$, the vertically adjacent holes touch each other when $\lambda=1/\varepsilon$ shown in Fig. 6(iii). In such cases, S_{max} is given by S_A in the calculated range of ε and λ.

In the above, We calculated S_{max} for various combinations of ε and λ. However, when the values for some other cases are required, we have to make interpolations with respect to two parameters, causing considerable errors in the results. In order to get reliable results for arbitrary values of the parameters, let us make power series formulae for S_{max}. Here we take into account for the behavior of S_{max} for both the problems. Then the behavior of S_{max} for

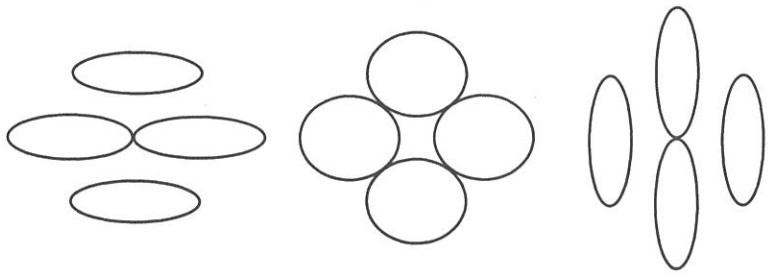

Fig. 6　Three extreme cases when adjacent holes touch each other (Problem (b))

Problem (b) depend on two ranges of ε, $\varepsilon \leq 1/3$ and $\varepsilon \geq 1/3$, as shown in Fig. 5(b), and different formulae in the two ranges are expected to give better accuracy.

Considering the above aspects, we have fitted power series to the analytical values of S_{max} for both the problems, and the following formulae are obtained:

(a) Square array of elliptical holes for Problem (a) ($\mu=1$)

$$S_{max}=1+\frac{\lambda^2}{1-\lambda}[0.2757-0.4126\varepsilon+0.1302\varepsilon^2-0.0376\varepsilon^3+\lambda(-0.2764+1.1465\varepsilon-1.4701\varepsilon^2+0.5137\varepsilon^3)$$
$$+\lambda^2(0.7736-2.5802\varepsilon+6.9170\varepsilon^2-2.2693\varepsilon^3)+\lambda^3(-1.0006+3.7412\varepsilon-11.9176\varepsilon^2+4.4548\varepsilon^3)$$
$$+\lambda^4(0.3349-2.2530\varepsilon+7.6266\varepsilon^2-3.2603\varepsilon^3)]$$
(mean error=0.05 percent)　(21)

(b) Zig-zag array of elliptical holes for Problem (b) ($\mu=1$)

For the range of $\varepsilon \leq 1/3$

$$S_{max}=1+\frac{\lambda^2}{1-\lambda}[1.8169+1.0436\varepsilon+0.5876\varepsilon^2+\lambda(-2.1638+1.1838\varepsilon-6.2676\varepsilon^2)$$
$$+\lambda^2(3.8925-9.3537\varepsilon+35.7642\varepsilon^2)+\lambda^3(-12.7934+3.9338\varepsilon-56.6534\varepsilon^2)$$
$$+\lambda^4(10.5138+1.9845\varepsilon+31.5175\varepsilon^2)]$$
(mean error=0.04 percent)　(22.1)

For the range of $\varepsilon \geq 1/3$

$$S_{max}=1+\frac{\lambda^2}{1-\frac{2\varepsilon\lambda}{\sqrt{\varepsilon^2+1}}}[1.7170+1.3916\varepsilon+0.2840\varepsilon^2+\lambda(-1.6954-0.0039\varepsilon-6.7001\varepsilon^2)$$
$$+\lambda^2(36.2512-83.2978\varepsilon+80.8250\varepsilon^2)+\lambda^3(-138.479+306.085\varepsilon-254.227\varepsilon^2)$$
$$+\lambda^4(129.517-298.641\varepsilon+246.157\varepsilon^2)]$$
(mean error=0.06 percent)　(22.2)

Values from eqns (21)-(22.2) are plotted in Fig. 5(a), (b) as dotted curves and dashed curves, respectively, showing close agreement with the analytical curves.

3. 3. Tensile stiffnesses and their formulae

Tensile stiffness factors $C=E^*/E_0$ defined by eqn (16) have been calculated for various values of ε and λ. Results for both the problems are shown by Tables 3(a) and 3(b), and are plotted in Figs. 7(a) and 7(b), respectively. E^*/E_0 decreases with increasing values of ε in both the problems. As compared with both problems, the magnitude of

decreasing E^*/E_0 for Problem (b) are lower than that for Problem (a).

The decrease of the tensile stiffness factor is highly correlated with the area of obstructing the stress flow by the elliptical holes. Thus, as holes exist in a material, the stress flow depends on the area of elliptical holes and dead zones which are area of obstructing it around holes. We assume that the rate of an effective area occupied in the used unit region, f_e, is given by the sum of the rate of the area of the elliptical hole, f, and the rate of the dead zone, q. f must be calculated from the area of the elliptical hole in the explicit form. But, as q is difficult to be calculated in the explicit form, we try to fit it by the power series of ε and λ on the base of the analytical values of E^*/E_0 for both the problems. Then, in the limiting case when $\varepsilon=0$ (cracks), q, which is the volume fraction of the fictitious circular holes enclosing the cracks, was useful in representing the tensile stiffnesses of the cracked solids[6]. We gave the parameter q on the basis of trial-and-error procedure as satisfied on the above considerations and being coincident curves of $\varepsilon\neq 0$ to the curve of $\varepsilon=0$ (cracks).

We determine the parameter f_e as follows:

(a) Square array of elliptical holes for Problem (a) ($\mu=1$)

$$f_e=f+q$$

$$f=\frac{\pi}{4}\lambda^2\varepsilon$$

$$q=\frac{\pi}{4}\lambda^2\left(1-\frac{1}{2}\varepsilon-\frac{1}{4}\lambda^2\varepsilon^2\right). \tag{23}$$

Table 3(a) E^*/E_0 for Problem (a) ($c/d=1$)

a/c	ρ/a									
	0	0.2	0.4	0.5	0.6	0.8	1.0	1.5	2.0	4.0
0.0	1.000	1.000	1.000	1.000	1.000	1.000	1.000	1.000	1.000	1.000
0.1	0.984	0.981	0.980	0.979	0.979	0.978	0.977	0.975	0.974	0.970
0.2	0.940	0.928	0.923	0.921	0.920	0.917	0.914	0.908	0.903	0.889
0.3	0.873	0.850	0.842	0.838	0.835	0.829	0.824	0.814	0.806	0.782
0.4	0.790	0.758	0.746	0.741	0.737	0.729	0.722	0.709	0.698	0.670
0.5	0.698	0.660	0.645	0.639	0.634	0.625	0.617	0.601	0.589	
0.6	0.602	0.560	0.543	0.537	0.531	0.520	0.512	0.495	0.483	
0.7	0.504	0.461	0.442	0.434	0.428	0.416	0.407	0.389	0.376	
0.8	0.405	0.360	0.338	0.330	0.322	0.310	0.300	0.282		

Table 3(b) E^*/E_0 for Problem (b) ($c/d=1$)

a/c	ρ/a											
	0	0.2	1/3	0.4	0.5	0.6	0.8	1.0	1.5	2.0	3.0	4.0
0.0	1.000	1.000	1.000	1.000	1.000	1.000	1.000	1.000	1.000	1.000	1.000	1.000
0.1	0.969	0.962	0.960	0.959	0.958	0.957	0.955	0.954	0.950	0.947	0.942	0.938
0.2	0.881	0.855	0.848	0.844	0.840	0.836	0.829	0.822	0.809	0.797	0.778	0.762
0.3	0.751	0.699	0.684	0.677	0.668	0.659	0.644	0.631	0.602	0.578	0.542	0.517
0.4	0.603	0.526	0.501	0.490	0.475	0.461	0.436	0.414	0.370	0.337	0.298	0.278
0.5	0.463	0.368	0.335	0.320	0.299	0.279	0.245	0.216	0.164	0.132		
0.6	0.349	0.245	0.204	0.185	0.160	0.137	0.100	0.072	0.028			

(b) Zig-zag array of elliptical holes for Problem (b) ($\mu=1$)

$$f_e=f+q$$

$$f=\frac{\pi}{2}\lambda^2\varepsilon$$

$$q=\frac{\pi}{2}\lambda^2\left(1-\frac{1}{2}\varepsilon+5\lambda^3\varepsilon^2\right). \tag{24}$$

The results are plotted in Figs. 8(a) and 8(b), taking f_e as the abscissa λ. We find that the E^*/E_0, f_e-curves in Figs. 8(a) and 8(b) lie in a narrow band than the E^*/E_0, λ-curves in Figs. 7(a) and 7(b), respectively. Therefore, f_e is useful in representing the tensile stiffnesses of the solids with the elliptical holes.

Considering the above aspects, we have fitted power series of f_e to the analytical values of E^*/E_0 for both the problems. The resulting expressions for the stiffness factor are as follows:

(a) Square array of elliptical holes for Problem (a) ($\mu=1$)

$$\frac{E^*}{E_0}=1-1.9931f_e+3.3372f_e^2-4.6333f_e^3+2.6823f_e^4 \quad \text{(mean error}=0.5 \text{ percent)} \tag{25}$$

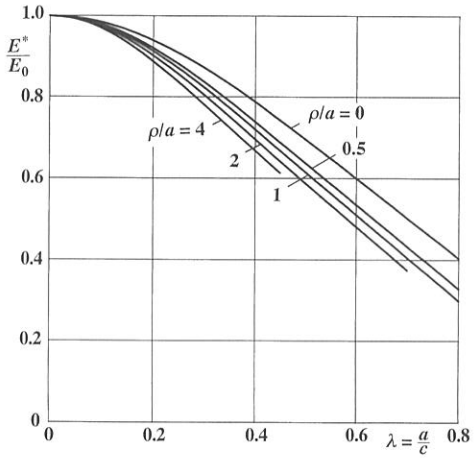

Fig. 7(a)　E^*/E_0, λ-relations for Problem (a) ($c/d=1$)

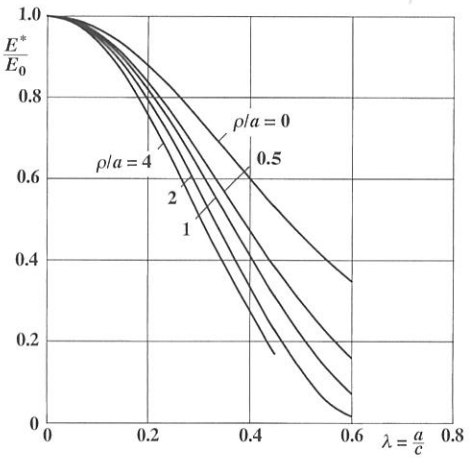

Fig. 7(b)　E^*/E_0, λ-relations for Problem (b) ($c/d=1$)

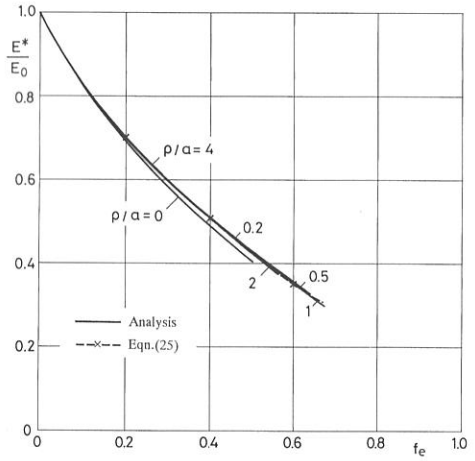

Fig. 8(a)　E^*/E_0, f_e-relations for Problem (a) ($c/d=1$)

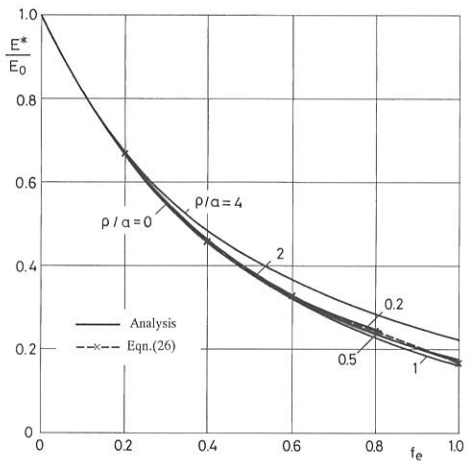

Fig. 8(b)　E^*/E_0, f_e-relations for Problem (b) ($c/d=1$)

(b) Zig-zag array of elliptical holes for Problem (b) ($\mu=1$)

$$\frac{E^*}{E_0}=1-2.0111f_e+1.9583f_e^2-0.7786f_e^3 \qquad \text{(mean error}=0.9 \text{ percent)} \tag{26}$$

Values of eqns (25) and (26) are plotted in Figs. 8(a) and 8(b) as dashed curves with cross marks, respectively, showing close agreement with the analytical values.

4. Concluding remarks

(1) A rectangular array and a zig-zag array of elliptical holes in solids under uniaxial tension were analyzed theoretically. Numerical results were given for dimensionless streesses S_A, S_B and a tensile stiffness E^*/E_0.

(2) In Problem (a), S_{max} occurred at point A. In Problem (b), S_{max} occurred at point A ($\theta=0$) in the most of λ without small and large values of ε, but it took place at some other point B ($\theta\neq0$) for intermediate values of ε and large values of λ, due to interference by the presence of obliquely located holes.

(3) E^*/E_0 decreased with increasing values of ε in both the problems. We gave the rate of the effective area, f_e, consisting of the sum of f, the rate of the area of elliptical hole, and q, the rate of dead zone, occupied in the used unit region. We confirmed that f_e was useful in representing the tensile stiffnesses of the solids with the elliptical holes.

(4) The analytical values of S_{max} and E^*/E_0 were fitted to reliable polynomial formulae for convenience of engineering applications.

Acknowledgements

I am indebted to Mr. William J. Underwood for helpful suggestions and comments in the paper.

References

(1) Makoto ISIDA, 'On the Stress Function in the Plate Problems of Elastic Body Containing a Free Elliptical Hole', Transactions of Japan Society for Mechanical Engineers, 21, 502-506.

(2) Makoto ISIDA, 'Method of Laurent Series Expansion for Internal Cracks Problem', *Methods of Analysis and Solutions of Crack Problems,* Mechanics of Fracture 1 (ed. Sih, G. C.), Noordhoff, 56-130.

(3) Makoto ISIDA, 'Effect of width and length on stress intensity factors of internally cracked plates under various boundary conditions', International Journal of Fracture Mechanics, Vol. 7, 1971, 301-316.

(4) Makoto ISIDA and Hiroshi NOGUCHI, 'Tension of a Plate Containing an Embedded elliptical crack', Engineering Fracture Mechanics, Vol. 20, 1984, 849-864.

(5) Makoto ISIDA and Hidenobu IGAWA, 'Analysis of a Zig-zag Array of Circular Holes in a Infinite Solid under Uniaxial Tension', International Journal of Solids and Structure, Vol. 27, No. 7, 1991, 849-864.

(6) Makoto ISIDA and Hidenobu IGAWA, 'Doubly-periodic Array and Zig-zag Array of Cracks in Solids under Uniaxial Tension', International Journal of Fracture, Vol. 53, 1992, 249-260.